Mechanism and regulation of the Lys6-selective deubiquitinase USP30

Malte Gersch[1], **Christina Gladkova**[#1], **Alexander F. Schubert**[#1], **Martin A. Michel**[1], **Sarah Maslen**[1], and **David Komander**[1,*]

[1]Medical Research Council Laboratory of Molecular Biology, Francis Crick Avenue, Cambridge, CB2 0QH, UK

[#] These authors contributed equally to this work.

Abstract

Damaged mitochondria undergo a specialised form of autophagy termed mitophagy, which is initiated by the ubiquitin kinase PINK1 and the E3 ligase Parkin. Ubiquitin-specific protease USP30 antagonises Parkin-mediated ubiquitination events on mitochondria and is a key negative regulator of mitophagy. Parkin and USP30 both display an unusual preference for assembly or disassembly, respectively, of Lys6-linked polyubiquitin, a chain type that has remained poorly studied. We here report crystal structures of human USP30 bound to mono- and Lys6-linked diubiquitin, which explain how USP30 achieves Lys6-linkage preference through unique ubiquitin binding interfaces. We assess the interplay between USP30, PINK1 and Parkin, and show that distally phosphorylated ubiquitin chains impair USP30 activity. Lys6-linkage specific affimers identify numerous mitochondrial substrates of this modification, and we show that USP30 regulates Lys6-polyubiquitinated TOM20. Our work provides insights into USP30 architecture, activity, and regulation, which will aid drug design against this and related enzymes.

Introduction

Protein ubiquitination regulates virtually all aspects of cellular biology, in particular protein homeostasis1–4. In addition to protein degradation via the proteasome system, ubiquitin also regulates lysosomal degradation of protein complexes and organelles through autophagy. The last few years have seen great leaps in our understanding of a specialised form of autophagy termed mitophagy, which targets damaged parts of mitochondria for autophagic clearance4–7.

Mitophagy ensues upon mitochondrial membrane depolarisation, which leads to stabilisation of the ubiquitin kinase PINK1 on the cytosolic face of the mitochondrial outer membrane (MOM)[8]. Here, PINK1 phosphorylates ubiquitin attached to mitochondrial proteins [9–13], and this recruits and activates the ubiquitin E3 ligase Parkin [14–17]. PINK1 phosphorylates and thereby fully activates recruited Parkin [18], which in turn hyperubiquitinates mitochondrial proteins on hundreds of sites [19] forming various types of ubiquitin linkages [12,20,21]. Mitochondrial (phospho)ubiquitination recruits mitophagy receptors as well as the autophagic machinery, and mitophagy proceeds [5,22,23]. This process occurs in response to endogenous mitochondrial damage [24], and can also be induced by chemical depolarisation [5,6]. Importantly, loss-of-function mutations in Parkin and PINK1 lead to early-onset autosomal recessive juvenile Parkinsonism (AR-JP), a neurodegenerative disorder arising from loss of dopaminergic neurons in the substantia nigra[5,25]. To date there are no treatments to stall AR-JP or other forms of Parkinson's disease.

Deubiquitinases reverse ubiquitin modifications and are thus important regulators of the ubiquitin system[26,27]. Parkin activity is reportedly counteracted by various deubiquitinases including USP8[20], USP15[28], USP30[29–31], and USP35[32]. Amongst those, USP30 is the only active deubiquitinase (DUB) known to be constitutively anchored in the MOM[33,34]. Importantly, Parkin and USP30 assemble[12,20] or disassemble[13,31], respectively, a similar set of ubiquitin linkages, sharing a preference for Lys6-linked chains. This ubiquitin chain type plays important yet obscure roles in mitophagy[21], the DNA damage response[4,35], and is assembled by bacterial effector E3 ligases[36,37], but direct substrates are unknown. The reported Lys6-linkage preference of USP30 is unusual for a USP domain deubiquitinase, which with few exceptions do not distinguish between different ubiquitin chain types[26,38,39]. Functionally, USP30 is a regulator of mitochondrial morphology[40] and mitophagy, and loss or reduced levels lead to increased mitochondrial turnover[29–31,41]. Inhibition of USP30 has consequently been proposed as a therapeutic means of re-establishing the balance between mitochondrial ubiquitination and deubiquitination in neurodegenerative disorders including Parkinson's disease[29].

To understand USP30 mechanistically and functionally, we performed structural and biophysical studies to reveal the molecular basis for USP30's Lys6 preference. We further reconstitute USP30 regulatory mechanisms in vitro, and show how even incomplete PINK1 kinase-mediated ubiquitin chain phosphorylation impacts USP30 activity. Finally, we exploit Lys6-linkage specific affimer reagents [42] to identify mitochondrial proteins that are modified with this linkage type during mitophagy, and show that USP30 regulates Lys6-polyubiquitination of TOM20.

Results

Optimising USP30 for crystallography

Human USP30 comprises 517 amino acids (aa) and consists of a mitochondrial intermembrane part (aa 1-35), a single transmembrane helix (aa 36-56) and a cytoplasmic catalytic domain (aa 57-517) that encodes the observed Lys6-preference[13,31]. A USP30 version with minimal boundaries (aa 64-502, USP30^{c2}, Fig. 1a, see Supplementary Table 1 for all constructs used in this study) cleaves Lys6-diubiquitin with preference over Lys11-

and Lys48-linked chains (Fig. 1b, Supplementary Fig. 1a), which was more pronounced when tetraubiquitin substrates were used (Fig. 1c, Supplementary Fig. 1b). Since this construct resisted crystallisation, we dissected the catalytic domain based on the previously reported USP Box annotation43 (Fig. 1a, d, Supplementary Fig. 1c, d, Supplementary Note 1), revealing multiple insertions in the catalytic domain. USP30 insertions are poorly conserved (Supplementary Fig. 1e, Supplementary Note 1), and are seemingly flexible as indicated by high deuterium uptake in hydrogen deuterium exchange mass-spectrometry (HDX-MS) measurements (Fig. 1d, Supplementary Fig. 1e). Removing a flexible, Pro-rich 74 residue insertion between box 4 and 5 resulted in poorly behaved protein (Supplementary Table 1). Modelling with known USP domain structures suggested that insert deletion might expose hydrophobic residues Phe348, Met350, Ile353 (Supplementary Fig. 2a). Mutation of those to hydrophilic residues eventually generated USP30^{c8} (Fig. 1a), that displayed improved expression levels, activity and solubility (Supplementary Table 1, see Supplementary Fig. 2b-f for construct characterisation). USP30^{c8} crystallised in complex with the ubiquitin-based suicide probe ubiquitin-propargylamine44 (Ub-PA), but low-resolution (3.6 Å) and twinning initially prevented structure determination.

Deletion of an additional, flexible 38-residue insertion between box 2 and 3 in USP30^{c13} further increased protein stability (Fig. 1a, d, Supplementary Fig. 2c), yet did not affect substrate preference (Fig. 1e, f). USP30^{c13} readily crystallised in complex with Ub-PA, resulting in a 2.3 Å USP30~Ub-PA structure that was used to phase the twinned USP30^{c8}~Ub-PA dataset (Fig. 1g, h, Supplementary Fig. 3a-c, Table 1). Moreover, mutation of catalytic Cys77 to Ala resulted in inactive USP30 (USP30^{c13i}, see Supplementary Table 1) that formed a complex with Lys6-diubiquitin on analytical gel-filtration (Supplementary Fig. 3d). A crystal structure of USP30^{c13i} in complex with Lys6-diubiquitin (USP30^{c13i}-Lys6-diUb) was determined at 2.8 Å resolution (Fig. 1i, Supplementary Fig. 3e, f, Table 1). Additional HDX-MS experiments confirmed that the insertion between box 2 and 3 is not involved in distal ubiquitin binding (Supplementary Fig. 4). Collectively, the structures reveal several unique features of USP30 and explain how USP30 achieves Lys6 preference.

Unusual features of USP30

Binding modes for the distal ubiquitin are identical in mono- and diubiquitin USP30 complexes (Fig. 1g-i). The overall orientation of ubiquitin is similar to previously determined USP~Ub complexes such as USP745 (Fig. 2a) or USP2146, but differs in how the ubiquitin C-terminus is guided into the active site. Most USP DUBs form near-identical and conserved backbone hydrogen bonds to all ubiquitin tail residues (Fig. 2a). USP30 lacks several of these interactions, and loss of three hydrogen bonds compared to other USPs such as USP7 (Fig. 2a, Supplementary Fig. 5a) suggests that binding of the distal ubiquitin has been selectively weakened. This explains complications with estimating USP30 K_M values for monoubiquitin substrates31,38, or K_d values for the interaction between inactive USP30 and fluorescent ubiquitin (Fig. 2b, Supplementary Fig. 5b, c); similar substrates bind other (inactive) USPs with nM to low µM affinities46,47 (Supplementary Fig. 5d).

USP30 is one of three USPs (with USP16 and USP45) that feature a serine as part of their catalytic triad (in USP30: Cys77, His452 and Ser477)43. In the USP30^{c13}~Ub-PA structure,

the Ser477 sidechain forms a hydrogen-bond with catalytic His452, implying a three-membered catalytic charge-relay system (Fig. 2c). As expected, Cys and His mutations abrogate USP30 activity, while Ser mutation to Ala, but also to Asn or Asp, that are usually found in USP DUBs43, reduce activity in both mono- and diubiquitin-based substrate cleavage assays (Fig. 2d, e, Supplementary Fig. 5e, f). Taken together, these data demonstrate functional importance for the unusual serine in the USP30 catalytic triad.

Explaining Lys6-linkage preference in USP30

DUBs achieve ubiquitin chain linkage preference by providing a defined binding site that positions the proximal ubiquitin with respect to the active site26. Indeed, fluorescently labelled Lys6-linked diubiquitin binds inactive USP30 with a K_d of ~4 μM, while other chain types show poor or no binding in the concentration range assessed (up to 60 μM diubiquitin) (Fig. 3a, Supplementary Fig. 6a, b). Unlabelled Lys6-linked diubiquitin binds with similar K_d in isothermal titration calorimetry experiments (Fig. 3b, Supplementary Figure 6c) and increases thermal stability of USP30, which is not observed for monoubiquitin or other diubiquitin linkages (Fig. 3c). This indicates that USP30 achieves its linkage preference through specifically interacting with Lys6-linked polyubiquitin.

The USP30 diubiquitin complex structure (Fig. 1i, 3d) explains this preferential binding, and reveals how the proximal ubiquitin interacts with USP30 in three areas (Fig. 3d-f):

The first and most prominent region contacted by the ubiquitin Phe4 patch localises to a hydrophobic surface on the USP30 palm subdomain that comprises conserved residues His445, catalytic His452 and in particular Trp475, which is not present in any other USP deubiquitinase43. Ubiquitin Phe4 and Thr12 thereby sit atop the catalytic triad and shield it from solvent.

The second region of the interface is mediated by the ubiquitin β1 and β2 strands and the Leu8 loop (Fig. 3d,f, Supplementary Fig. 6d), which contact USP30 loops from thumb (residues 71-74) and palm (β12-β13 hairpin) subdomains, forming five hydrogen bonds.

Thirdly, several interactions surround the ubiquitin Lys6 side chain that reaches into the active site (Fig. 3d,f). The ubiquitin isopeptide bond is fully engulfed by USP30, and residues from the thumb subdomain (Glu159, Asn75) reach over the ubiquitin binding channel to contact the palm subdomain (Fig. 3d, e, Supplementary Fig. 6e, f). This shields the isopeptide and catalytic centre from solvent, but also stretches out the diubiquitin, which adopts a distinct conformation as compared to its compact solution structure37 (see Supplementary Fig. 7).

The distal ubiquitin interaction is considerably stronger as compared to proximal ubiquitin binding (1652 Å^2 vs. 535 Å^2 buried surface area, 49 vs. 10 polar interactions, solvation free energy –6.4 vs. –2.0 kcal/mol), but the proximal ubiquitin binding site provides the observed linkage preference. Notably, catalytic Ser477 contributes to the proximal interface, and specificity characterisations reveal that USP30 S477D has lost Lys6-linkage preference (Fig. 3g, Supplementary Fig. 6g, h). Similarly, USP30 mutations of His445 or Trp475 that disrupt the Phe4 binding interface of the proximal ubiquitin are less active and, importantly, less

specific as compared to wild-type USP30 (Fig. 3h, Supplementary Fig. 8). Hence, mutations in the proximal ubiquitin binding site reduce the observed linkage preference of USP30.

Together, this offers a straightforward model for how USP30 achieves its Lys6-preference, namely by balancing distal and proximal ubiquitin interactions such that Lys6-linked chains are bound preferentially (Fig. 4a). The presence of a proximal ubiquitin binding site distinguishes USP30 from other USP enzymes, which commonly comprise only a high-affinity distal ubiquitin binding site; consequently, many lack pronounced linkage preference[26,38,39] (Fig. 4b). The only other case where USP linkage specificity is present and molecularly understood is CYLD, which prefers Lys63- and Met1-linked chains [48–50]. CYLD uses a mechanism that is conceptually similar to USP30 (Fig. 4c), but which differs at the molecular level. Structures of CYLD with Lys63- and Met1-linked diubiquitin revealed how a divergent domain architecture gives rise to distinct and CYLD-specific ubiquitin binding modes[50]. Superposition of USP30 and CYLD complexes shows how especially the proximal binding sites diverge, to enable either enzyme to target distinct linkage types (Fig. 4d-f, Supplementary Fig. 9). Whereas USP30 uses an interface embedded into its USP domain, CYLD utilises an inserted β-sheet protruding out of its catalytic domain to position the proximal ubiquitin (Fig. 4a, c). Further specificity and structural studies of USP enzymes will likely reveal additional features of binding sites for a proximal ubiquitin or substrate protein.

Ubiquitination of USP30 by Parkin

USP30 antagonises mitophagy[29,31], and the key signalling molecules in mitophagy, the E3 ligase Parkin and the ubiquitin kinase PINK1, may be able to regulate USP30 [13,29,31]. Parkin ubiquitinates USP30 in cells which may lead to its degradation[29]. In vitro reconstitution of USP30 ubiquitination by phosphorylated Parkin (Fig. 5a, Supplementary Fig. 10a) revealed monoubiquitination on Lys235 and Lys289 at the tip of the fingers subdomain, and on Lys310 in the distal ubiquitin binding site (Fig. 5b, Supplementary Data Table 2), matching sites previously found in cells[29,31]. Interestingly, although Parkin assembled ubiquitin chains in these reactions, USP30 appeared to be predominantly monoubiquitinated (Fig. 5a, Supplementary Fig. 10a). Monoubiquitinated forms of USP30 have been reported in cells, and were, compared to other Parkin substrates, relatively stable[30]. To test whether monoubiquitination affects USP30 activity, we had to overcome the challenge that USP30 auto-deubiquitinates in vitro. We hence modified USP30 with a ubiquitin mutant, Ub F4R, that was efficiently attached to USP30 by Parkin, but which prevented auto-deubiquitination as USP30 was no longer able to bind it for structural reasons (Fig. 5c, Supplementary Fig. 10b, c). Surprisingly, monoubiquitinated USP30 had indistinguishable cleavage activity towards ubiquitin-KG-TAMRA as compared to unmodified USP30 (Fig. 5c). Hence, while Parkin-mediated monoubiquitination of USP30 can be reconstituted in vitro, the impact on USP30 function is less clear: monoubiquitinated USP30 is active and unlikely to be directly targeted for proteasomal degradation.

Indirect regulation of USP30 by PINK1

PINK1 generates Ser65-phosphorylated ubiquitin (hereafter phosphoubiquitin), and phosphorylated Lys6-diubiquitin is a poor USP30 substrate[13]. However, Parkin is unable to

assemble phosphoubiquitin into chains13 and only 20% of mitochondrial ubiquitin is phosphorylated upon chemical depolarisation21. Although we and others had shown that polyubiquitin can be phosphorylated by PINK113,51, we wondered whether PINK1 may target distinct chain types with different kinetics. We hence characterised Lys6, Lys11, Lys48 and Lys63 di- and tetraubiquitin phosphorylation in an intact protein mass spectrometry-based assay (Fig. 6a-c). Time course analysis revealed similar rates for the first phosphorylation event in all chain types, but we noticed that phosphorylation of Lys6-linked diubiquitin displayed biphasic behaviour with the second phosphorylation event occurring slower that the first one (Fig. 6a). Analysis of asymmetric Lys6 diubiquitin phosphorylation revealed that this chain type is first phosphorylated on the distal ubiquitin (Supplementary Fig. 11a). This is consistent with the conformation of Lys6-linked chains in solution37, in which Ser65 is fully exposed only on the distal ubiquitin, likely explaining the delayed phosphorylation kinetics on the proximal ubiquitin molecules in Lys6-linked di- or tetraubiquitin (Fig. 6a-c). This behaviour is in contrast to Lys63-linked chains, which are phosphorylated rapidly on each ubiquitin molecule (Fig. 6b, c); more compact Lys11- and Lys48-linked chains receive a second phosphorylation with intermediate rates. Together this suggests that Lys6-linked chains on mitochondria may be predominantly distally phosphorylated, whereas Lys63-linked chains may contain internal phosphoubiquitin moieties. These findings may help explain why mitochondrial ubiquitin is only partially phosphorylated.

Superposition of phosphoubiquitin onto the ubiquitin moieties bound to USP30 revealed that phosphate groups on either ubiquitin in the USP30-Lys6-diUb complex would be adjacent to negatively charged USP30 residues (Fig. 6d, Supplementary Fig. 11b). Structural characterisation revealed that Ser65-phosphorylated ubiquitin exists in a slowly exchanging equilibrium between a 'common' ubiquitin conformation and a conformation in which the ubiquitin C-terminus is retracted13,52. The latter conformation is structurally incompatible with productive binding in the distal ubiquitin binding site of USP deubiquitinases13. USP30 hydrolyses phosphorylated ubiquitin-KG-TAMRA with ~8-fold lower efficiency (Fig. 6e, Supplementary Fig. 11c-e), and phosphorylation of monoubiquitinated inactive USP30 consistently impaired deubiquitination by active USP30 (Fig. 6f, g, Supplementary Figure 12a). This suggests that substrates where phosphoubiquitin would engage the distal ubiquitin binding site are more resistant to deubiquitination by USP30. This extends to Lys6-, Lys11-, Lys48- and Lys63-linked diubiquitin, all of which are worse substrates for USP30 when phosphorylated (Fig. 6h) 13 as they would engage the distal ubiquitin binding site.

To investigate in more detail whether both distal and proximal Ub binding sites of USP30 are susceptible to regulation through phosphoubiquitin, we assembled Lys6-linked diubiquitins with Ser65 phosphorylation exclusively on the distal, the proximal or both ubiquitin moieties (Supplementary Fig. 12b). Gel-base kinetics showed that phosphorylation of the distal, but not the proximal ubiquitin resulted in diminished USP30 activity (Fig. 6i, j). Strikingly however, a singly phosphorylated Lys6-tetraubiquitin species with one phosphoubiquitin at the distal tip was similarly protected from USP30-mediated hydrolysis as compared to an almost fully phosphorylated tetraubiquitin (Fig. 6k). Hence, despite

containing unphosphorylated Lys6-linkages, a singly phosphorylated Lys6-linked chain becomes a poor USP30 substrate.

This can be explained structurally. Like other USP enzymes37, USP30 is a compulsory exo-DUB towards Lys6-linkages, i.e. it hydrolyses this chain type exclusively from the distal end (see 26, discussion in Supplementary Fig 1b legend). Lys6 of the distal ubiquitin is shielded by the fingers subdomain in the distal ubiquitin binding site (Supplementary Fig. 10b), disallowing chain extension on Lys6; as a result, only the unmodified tip of Lys6-linked chains can interact with a USP, explaining exo-DUB activity. Phosphorylation of this distal ubiquitin by PINK1 (see above) hence protects the entire Lys6-linked chain from USP30-mediated hydrolysis.

Role of USP30 in regulating mitochondrial ubiquitination events

We next considered how our biochemical and structural insights into USP30 could be linked with its physiological context. USP30 is anchored on the surface of mitochondria, and only 10 residues bridge the transmembrane helix and the start of the catalytic domain. This likely imposes restrictions for substrate accessibility. Indeed, USP30 regulates numerous ubiquitination sites on MOM proteins29,30,32,40, which indicates that USP30, in addition to targeting polyubiquitin chains, can hydrolyse the isopeptide bond between substrate and the first ubiquitin. The accessible active site geometry of the USP domain, whilst designed to discriminate ubiquitin linkages, would allow for this substrate promiscuity.

The emergence of Lys6-polyubiquitin on mitochondria has been linked to Parkin activation upon mitochondrial damage12,20,21,31. Mitochondrial Lys6-linked polyubiquitin increases five-fold when USP30 is deleted while other chain types remain unchanged31. This suggests that the preferred hydrolysis of Lys6-linkages by USP30 contributes to shaping the polyubiquitin pool on mitochondria. However, it is not known which MOM proteins are modified with Lys6-linkages, and the abundance of Lys6-linkages in cells is very low (between 0.5 and 2% of all linkages53,54). Linkage-specific antibodies can show that proteins are modified with a particular chain type55–57, but are not available for the Lys6-linkage. Recently developed chain linkage specific affimers42 allowed us to investigate Lys6-linked ubiquitin chains in a mitochondrial context. Enrichment of Lys6-ubiquitinated proteins with the affimer from HeLa Flp-In T-REx cells that inducibly express wild-type Parkin12 facilitated the detection of ubiquitinated forms of MOM proteins TOM20, VDAC1, MFN2, MIRO1 and CISD1 (Fig. 7a, Supplementary Fig. 13a) which are known substrates of Parkin19, in a Parkin- and depolarisation-dependent manner. Consistent with the requirement for a Lys6-linkage, the monoubiquitinated forms of these proteins were not enriched (Fig. 7a). Interestingly, Lys6-polyubiquitin signals of TOM20, but not of other MOM proteins tested, were increased upon knockdown of USP30 (Fig. 7b, c, Supplementary Fig. 13b, c). Moreover, expression of USP30 or catalytically inactive USP30 C77A led to a decrease or increase of TOM20 Lys6-ubiquitination, respectively (Fig. 7d, e). In addition, overexpression of active USP30 resulted in reduced levels of Lys6-ubiquitinated forms of other proteins as well (Fig. 7d, Supplementary Fig. 13d, e). Together, affimer based detection confirms that Lys6-linked chains become abundant on mitochondrial proteins 31,42, and reveal direct substrates for this unstudied ubiquitin modification. Lys6-linkages

on TOM20 correlate with levels of USP30, which may represent a direct read-out of USP30 cellular activity.

Discussion

We here reveal how USP30, the only human DUB directly inserted in the outer mitochondrial membrane, achieves a preference for the unstudied Lys6-linked ubiquitin chain type. We further show how USP30 is regulated by PINK1 and Parkin that initiate mitophagy, and how it regulates the deubiquitination of mitochondrial proteins including TOM20 during mitophagy. The identification of substrates for Lys6-polyubiquitin modification using new affinity tools for this linkage type supports important roles of this chain type, in addition or in conjunction with phosphoubiquitin, as a mitophagy-inducing signal[21]. Moreover, it was previously shown that cells expressing a non-ubiquitinatable form of TOM20 do not efficiently undergo mitophagy[29], which was based on findings that USP30 directly regulates TOM20 ubiquitination (i.e. it cleaves the bond between TOM20 and the 'first' ubiquitin). We here extend this by showing that TOM20 is modified with Lys6-linked chains in a Parkin-dependent manner. USP30 interacts directly with TOM20 (ref.[30]) and stabilises it during mitophagy induction[29,30], while USP30 knockdown increases TOM20 Lys6-ubiquitination. Hence, it is tempting to speculate that USP30 regulates mitophagy at least in part via regulating TOM20 ubiquitination (Fig. 7f). It will now be important to understand the special role of TOM20 and how its Lys6-ubiquitination mechanistically regulates mitophagy, and which other proteins behave similarly to TOM20 during mitophagy. There could be multiple reasons why Lys6-modifications of other proteins are seemingly not regulated by USP30 knockdown. For example, USP30 may require physical proximity to its substrates[30], or appropriate chain architectures to be efficient. Also, PINK1 activity may protect some of the observed ubiquitination events from USP30 cleavage.

Indeed, it seems counterintuitive that USP30 can antagonise mitophagy since it is ubiquitinated by Parkin[29] and potentially degraded, and also seemingly unable to efficiently process PINK1-induced phosphoubiquitin signals (Fig. 6). Our and previous data[29,30] seem consistent with a model in which USP30 may not act in a negative feedback loop to stop mitophagy after initiation, but where it constitutively counteracts mitophagy initiation (and possibly other mitochondrial ubiquitination events). In such model, USP30 may keep mitochondrial ubiquitination below a threshold that is required to efficiently trigger mitophagy. Activation of PINK1 and Parkin would imbalance this equilibrium, by depositing large amounts of (poly)ubiquitin and phosphoubiquitin to overcome USP30 activity. This scenario explains data obtained under depolarisation conditions where USP30 knock-down or loss increases mitophagy [29–31]. In a physiological scenario, mitochondria undergo fission and fusion processes and upon localised damage are able to isolate and degrade affected parts of the mitochondrial network. USP30 here may be able to respond locally to the PINK1/Parkin status and it is tempting to speculate that this may allow USP30 to contribute to defining the spatial extend of the mitophagised area (Supplementary Figure 14), for example by regulating concomitant fission/fusion events [40]. These cell-biological questions are not easy to address, and will require detailed high-resolution assessment of mitophagy mechanisms.

Taken together, our data contribute to explaining how USP30 can act as a brake on mitophagy. As previously noted, this makes USP30 an attractive drug target, in particular in conditions in which mitophagy initiation is compromised, such as in patients with Parkin mutations. An inhibitor of USP30 may here lower the threshold for mitophagy induction, which has been shown to proceed in cells expressing very low Parkin levels that nonetheless rely on mitochondrial ubiquitin22. The here reported structural differences between USP30 and other USP-family DUBs improve the prospects of finding USP30-specific inhibitors, which may benefit patients with early onset Parkinson's disease, but may also be useful in other contexts of mitochondrial dysfunction.

Online Methods

Cloning and constructs

cDNA of human USP30 (Uniprot entry Q70CQ3) was obtained from GeneArt Gene Synthesis with codon-optimization for bacterial expression. All constructs (see Supplementary Table 1) were cloned into pOPIN vectors58 using the In-Fusion HD Cloning Kit (Takara Clontech). Site-directed mutagenesis was carried out using the QuikChange method or with overlap extension PCR59.

USP30 constructs were cloned with an N-terminal His$_6$ tag, a 3C protease cleavage site, a glutathione S-transferase (GST) tag and another 3C protease cleavage site followed by the protein sequence. The chosen purification strategy exploits the ability of untagged human USP30 to weakly bind to Ni-NTA resin facilitating separation from free GST.

Point-mutations were introduced into construct 2 (boundaries 64–502, no deletions or additional mutations) unless noted otherwise.

Protein expression and purification

E. coli Rosetta2 pLacI cells (Novagen) were chemically transformed with expression vector and subsequently grown in 2xTY media supplemented with appropriate antibiotics to an optical density (OD$_{600}$) of 0.8–1.0 at 30°C. After cooling down to 18°C for ~1 h, expression was induced by addition of 0.5 mM isopropyl-β-D-1-thiogalactopyranoside (IPTG) and cells were kept shaking for 18 h at 18°C. After harvest by centrifugation, cell pellets were flash frozen in liquid nitrogen and stored at –80°C.

Cells were resuspended in lysis buffer (50 mM sodium phosphate pH 8.0, 300 mM sodium chloride, 5 mM β-mercaptoethanol, 20 mM imidazole) supplemented with 2 mg/mL lysozyme, 0.2 mg/mL DNaseI and one EDTA-free Complete Protease Inhibitor Cocktail tablet (Roche). The suspension was then incubated on ice for 20 min, sonicated for 5 min (10 s on / 10 s off, 62 W), cleared by centrifugation at 22,500xg for 30 min at 4 °C and filtered through a 0.45 μm filter.

All following purification steps were carried out on an Äkta Explorer system (GE Healthcare) at 4°C. For affinity chromatography, lysate was loaded onto a pre-equilibrated 5 mL HisTrap Fast Flow column (GE Healthcare), washed with 10 column volumes (CV) of lysis buffer, washed with 12 CV of lysis buffer supplemented with additional 20 mM

imidazole and then eluted with a linear gradient over 5 CV into elution buffer (50 mM sodium phosphate pH 8.0, 300 mM sodium chloride, 5 mM β-mercaptoethanol, 500 mM imidazole). Protein-containing fractions were pooled, supplemented with His$_6$-tagged 3C protease and dialysed against lysis buffer at 4°C for 4–24 h. The next round of affinity purification enriches untagged human USP30 on Ni-NTA resin while free GST is separated out through the flow through. The dialysed solution was diluted two-fold with lysis buffer and passed through a 5 mL HisTrap FastFlow column. After washing with lysis buffer for 10 CV, USP30 was eluted as described above. Protein containing fractions were pooled and dialysed at 4°C into buffer A (25 mM Tris pH 8.5, 50 mM NaCl, 5 mM DTT) for 4–24 h. Samples were then subjected to anion-exchange chromatography on a 6 mL Resource Q column (GE Healthcare) with linear elution into buffer B (25 mM Tris pH 8.5, 500 mM NaCl, 5 mM DTT) and final size-exclusion chromatography (HiLoad 16/600 Superdex 75 pg, GE Healthcare) in buffer C (20 mM Tris pH 8.0, 100 mM NaCl, 5 mM DTT). Purity of peak fractions was assessed by SDS-PAGE before pooling, concentrating at 4°C / 3,200 xg in spin concentrators (10 kDa MWCO, Viva spin) and flash freezing in liquid nitrogen. All protein concentrations were determined by absorption at 280 nm unless noted otherwise. USP2146, GST-tagged *Ph*PINK114, full-length *Hs*Parkin14, ubiquitin and ubiquitin chains60 were expressed, purified and assembled as described previously.

Assembly of Ub-propargylamine suicide probe44

Ub(1-75)-MesNa was prepared as described previously61. 0.7 g of propargylamine hydrochloride (Aldrich, P5091) were dissolved in 7 mL of buffer D (20 mM Hepes, 50 mM sodium acetate, pH 6.5, 75 mM sodium chloride), supplemented with 490 μL of 4 M sodium hydroxide, and added to 6 mL of 600 μM Ub(1-75)-MesNa in buffer D. The final pH of the reaction mixture was between 8.0 and 8.5. Following incubation at room temperature for 3 h, completion of the reaction was observed by intact protein mass spectrometry (expected mass: 8,544.8 Da, mass found: 8,544.1 Da). The reaction mixture was then concentrated to 2.5 mL in a spin concentrator (3 kDa MWCO, Amicon Ultra) for size-exclusion chromatography (HiLoad 16/600 Superdex 75 pg, GE Healthcare) in buffer D to yield ubiquitin(1-75)-propargylamine suicide probe (Ub-PA).

Modification of USP30 with Ub-PA suicide probe

Following the second affinity purification step, USP30 was mixed with 1.3 equivalents of Ub-PA, dialysed into buffer B and further purified by anion-exchange and size-exclusion chromatography as described above.

Crystallisation

Crystallisation experiments were carried out at 18°C in 96-well sitting-drop vapour diffusion plates in MRC format (Molecular Dimensions) and set up using nano-litre robotics (Mosquito HTS, TTP Labtech). Typical drop ratios of protein solution to reservoir of 200 nL + 200 nL and 500 nL + 500 nL were used for coarse screening and fine screening, respectively. Streak-seeding crystallisation experiments were set up in 24-well sitting drop vapour diffusion plates with a protein solution to reservoir ratio of 2 μL + 2 μL.

Initial crystals of USP30^{c8}~Ub-PA (9.0 mg/mL) were found in 0.02 M magnesium chloride, 0.1 M Hepes pH 7.5, 22% (w/v) polyacrylic acid (PAA) 5,100 Na. Additive screening (Hampton HR2) and streak-seeding with crushed crystals grown in 20% (w/v) PAA 5,100 Na, 100 mM Hepes pH 8.0, 2.5% (v/v) glycerol into drops of the same condition yielded large (200x240x150 μm^3) hexagonal crystals.

Crystals of USP30^{c13}~Ub-PA (10.7 mg/mL) grew in 10% (w/v) PEG 20,000, 0.1 M sodium citrate pH 5.4, 0.2 M Li$_2$SO$_4$ as thin needles (150x30x30 μm^3).

Initial crystals of a non-covalent complex of inactive USP30^{c13i} with Lys6-linked diubiquitin (1:1.15 eq, 12.5 mg/mL total protein concentration) grew in 0.7 M sodium citrate, 0.1 M Tris pH 8.5. Small needles (50x10x10 μm^3) of diffraction-quality were obtained in 0.73 M sodium citrate, 0.1 M Hepes pH 7.0 in 600 + 400 μL drops.

Crystals were soaked in mother liquor supplemented with 25–30% (v/v) glycerol before vitrification in liquid nitrogen.

Data collection, structure determination and refinement

Diffraction data were collected at the Diamond Light Source, Harwell, UK, at 100 K at beamlines I04-1 (wavelength: 0.9282 Å), I02 (wavelength: 0.9795 Å) and I24 (wavelength: 0.9686 Å) for the 3.6 Å, 2.3 Å and 2.8 Å datasets, respectively. Diffraction images were indexed and integrated using XDS[62] or DIALS[63], and scaled using AIMLESS[64] (Wilson B-factors: 136.3 Å^2, 31.8 Å^2 and 49.3 Å^2). The USP30^{c13}~Ub-PA structure was determined from the 2.3 Å dataset by molecular replacement using PHASER[65] with a chainsaw[66] model derived from the structure of USP2 covalently bound to Ub (PDB 2HD5[47]). Phases for the USP30^{c13i} + Lys6-diUb complex were obtained by molecular replacement using the coordinates of the 2.3 Å USP30^{c13}~Ub-PA dataset and another copy of C-terminally truncated ubiquitin (residues 1-72, PDB 1UBQ[67]). The twinned 3.6 Å dataset of USP30^{c8}~Ub-PA was solved in space group $P6_5$ with two molecules per asymmetric unit by molecular replacement using the 2.3 Å structure of USP30^{c13}~Ub-PA as search model (twin law: h, k, l = k, h, –l; twin fractions: 0.52 / 0.48). The final refinement of the 3.6 Å structure was carried out with external restraints using ProSmart[68] against the geometry of the 2.3 Å structure. The resulting 3.6 Å map allows for clear tracing of the polypeptide chain and informs on the presence/absence of loops but has little features with regards to side chain conformations. Models were built in Coot[69] and refined in PHENIX[70] or Refmac[71] in iterative rounds of manual inspection and building, using simulated annealing and Phenix elbow-derived geometry restraints for the PA warhead where appropriate. Both needle-shaped crystal forms showed pronounced susceptibility to radiation damage as evident from the merging statistics. Model quality was assessed using the Molprobity analysis tools (3.6 Å USP30^{c8}~Ub-PA structure: Ramachandran statistics (favoured/allowed/outliers): 94.6/5.1/0.3%, Rotamer outliers: 4.9, Clashscore: 7.1; 2.3 Å USP30^{c13}~Ub-PA structure: Ramachandran statistics (favoured/allowed/outliers): 95.4/4.3/0.3%, Rotamer outliers: 3.5, Clashscore: 6.7;. 2.8 Å USP30^{c13i} + Lys6-diUb structure: Ramachandran statistics (favoured/allowed/outliers): 97.0/3.0/0.0%, Rotamer outliers: 2.4, Clashscore: 5.0). Final data collection and refinement statistics are summarised in Table 1.

Fluorescence polarisation assays

Measurements were performed with a PheraStar plate reader (BMG Labtech), equipped with an optic module for FlAsH (λ_{ex} = 485 nm, λ_{em} = 520 nm) or TAMRA (λ_{ex} = 540 nm, λ_{em} = 590 nm) fluorophore detection. Data were recorded in black, round-bottom, non-binding surface 384-well plates (Greiner) at 25 °C in 20 μL (kinetics) or 15 μL (binding experiments). For kinetics, typically one read per min over 60 min was carried out, with 0.1 μM of fluorescent substrate. For binding assays typically 10 reads per well were recorded with 70 nM of fluorescently labelled Ub probe (4 nM of Ub-KG-TAMRA were used for the USP21 (C221A) binding experiment). Raw data were referenced against the polarisation values as determined by a cuvette-based spectrofluorometer (TAMRA-KG (50 mP), Ub-KG-TAMRA (160 mP) and Lys6-diUb-FlAsH (335 mP)) and were then converted into anisotropies (mA). All experiments were performed in triplicate and in at least two independent experiments. Kinetic experiments were carried out in PBS (phosphate-buffered saline, pH 7.4) + 5 mM DTT + 0.05 mg/mL BSA. Binding experiments were carried out in 20 mM Tris pH 8.0, 100 mM NaCl, 5 mM DTT and 0.05 mg/mL BSA. Data were analyzed in the PheraStar Data Analysis program, Microsoft Excel and GraphPad Prism. For kinetic experiments, technical triplicates were averaged, background-corrected by subtracting the linear slope of the KG-TAMRA control well or the final part of the curve, and subjected to non-linear curve fitting to extract the exponential decay in fluorescence (Fit: Plateau followed by one-phase exponential decay). The observed rate constants obtained thereby were then plotted over the enzyme concentration, yielding catalytic efficiencies as the slopes (identical to the k_{cat}/K_M ratio). For binding assays, anisotropies of replicate wells were averaged and plotted in GraphPad Prism for non-linear curve fitting to determine the affinity constant, K_d (Fit: One-site binding – Total).

diUb/tetraUb cleavage assays

Cleavage of diubiquitin (diUb) and tetraubiquitin (tetraUb) proteins was followed by SDS-PAGE and Coomassie or silver staining. 50 μL reactions were set up by mixing 25 μL of 0.5–4.0 μM USP30 (2x) and 25 μL of diUb (3-8 μM, 2x) or tetraUb (4 μM, 2x). PBS + 5 mM DTT + 0.05 mg/mL BSA was used as buffer. Reactions were incubated at 37ºC. Aliquots were taken at indicated time points by mixing 10 μL with 5 μL of SDS sample buffer. In the diUb panel comprising all eight linkages, Lys27-diUb was chemically synthesised (UbiQ), whereas all other substrates were enzymatically assembled using wild-type ubiquitin.

For cleavage assays with phosphorylated diubiquitin (Fig. 6h), samples were diluted in 20 mM Tris pH 8.0, 100 mM NaCl, 5 mM DTT, 10 mM ATP, 10 mM MgCl$_2$ and were then treated with *Ph*PINK1 for 720 min. Incorporation of two phosphate groups in Lys11-, Lys48- and Lys63-linked diubiquitin was confirmed by LC-MS.

For gel-based kinetics, assays were carried out as described above and as labelled in the raw data shown in the Supplementary Data Set 1. Gels were Coomassie stained (Instant Blue, Expedeon), images of the gels were converted to greyscale and monoUb band intensities were quantified with ImageJ. Background subtraction was carried out for each band using an identically sized, empty area above the band. Intensities were obtained from multiplying the

background-corrected mean signal with the area size. Plotting of the intensity values over time yielded slopes that were used as relative activity measures. Only data in the linear range of the time course were used. Data from the independent experiments were normalised to their respective Lys6-diUb assay and then averaged. Catalytic efficiencies were calculated by quantifying the monoUb bands relative to the diUb bands, taking the different USP30 concentrations into account.

Hydrogen–deuterium exchange mass spectrometry (HDX-MS)

Deuterium exchange reactions of USP30[c2], USP30[c8] and USP30[c8]~Ub-PA were initiated by diluting the samples in D_2O (99.8% D_2O ACROS) in 20 mM Tris, 50 mM NaCl, 1 mM TCEP pH 7.5 buffer to give a final D_2O percentage of 90%. Deuterium labelling was carried out for 3 seconds on ice in triplicate. The labelling reaction was quenched by the addition of chilled 2.4% (v/v) formic acid in 2 M guanidinium hydrochloride and immediately frozen in liquid nitrogen. Samples were stored at –80°C prior to analysis.

The quenched protein samples were rapidly thawed and subjected to proteolytic cleavage by pepsin followed by reversed phase HPLC separation. Briefly, the protein was passed through an Enzymate BEH immobilised pepsin column, 2.1 x 30 mm, 5 μm (Waters) at 200 μL/min for 2 min and the peptic peptides were trapped and desalted on a 2.1 x 5 mm C18 trap column (Acquity BEH C18 Van-guard pre-column, 1.7 μm, Waters). Trapped peptides were subsequently eluted over 12 min using a 5–36% gradient of acetonitrile in 0.1% (v/v) formic acid at 40 μL/min. Peptides were separated on a reverse phase column (Acquity UPLC BEH C18 column 1.7 μm, 100 mm x 1 mm, Waters). Peptides were detected on a SYNAPT G2-Si HDMS mass spectrometer (Waters) acquiring over a m/z of 300 to 2000, with the standard electrospray ionization (ESI) source and lock mass calibration using [Glu1]-fibrino peptide B (50 fmol/μL). The mass spectrometer was operated at a source temperature of 80°C and a spray voltage of 2.6 kV. Spectra were collected in positive ion mode.

Peptide identification was performed by MSe[72] using an identical gradient of increasing acetonitrile in 0.1% (v/v) formic acid over 12 min. The resulting MSe data were analysed using Protein Lynx Global Server software (Waters) with an MS tolerance of 5 ppm.

Mass analysis of the peptide centroids was performed using DynamX software (Waters). Only peptides with a score >6.4 were considered. The first round of analysis and identification was performed automatically by the DynamX software, however, all peptides (deuterated and non-deuterated) were manually verified for the correct charge state, presence of overlapping peptides, and correct retention time. Deuterium incorporation was not corrected for back-exchange and represents relative, rather than absolute changes in deuterium levels. Changes in H/D amide exchange in any peptide may be due to a single amide or a number of amides within that peptide.

Parkin/USP30 ubiquitination assays and mass spectrometry

Ser65 phosphorylated *Hs*Parkin (pParkin) was generated by phosphorylating *Hs*Parkin with GST-tagged *Ph*PINK1, which was then removed by incubation with Glutathione-S-Sepharose Beads (Amintra) followed by size exclusion chromatography (HiLoad 16/600 Superdex 75 pg) and anion-exchange chromatography (Resource Q, GE Healthcare). Spin-

filtered pParkin (4 μM) was incubated for 2 h at 37 ºC with indicated spin-filtered USP30 constructs (4 μM) in the presence of mouse E1 (0.2 μM), UBE2L3 (2 μM), ubiquitin (120 μM, S65A) and (where indicated) Ser65 phosphorylated ubiquitin (pUb, 12 μM) in reaction buffer (50 mM Tris pH 8.5, 200 mM NaCl, 10 mM $MgCl_2$, 10 mM ATP, 10 mM DTT).

Reactions were quenched using LDS buffer containing β-mercaptoethanol and iodoacetamide. Proteins were resolved on 4-12% NuPAGE gradient Bis-Tris gels (Invitrogen) and transferred to a nitrocellulose or PVDF (only for ubiquitin blot in Supplementary Fig. 10a) membrane using the Trans-Blot Turbo system (Bio-Rad). Membranes were blocked in a 5% (w/v) milk solution in PBS-T (PBS + 0.1% (v/v) Tween-20) for 30 min and incubated overnight at 4 °C with a primary antibody recognizing either USP30 (HPA016952, Atlas Antibodies), ubiquitin (Ubi-1, NB300-130, Novus Biologicals) or pSer65 ubiquitin (ABS1513-I, Millipore). The membrane was then washed with PBS-T, incubated for 1 h at room temperature with anti-rabbit or anti-mouse IgG-HRP (NA934V or NXA931, GE Healthcare) in 5% (w/v) milk in PBS-T, washed in PBS-T, visualised with Amersham Western Blotting Detection Reagent (GE Healthcare) and imaged using a ChemiDocTM Touch Imaging System (Bio-Rad).

For mass spectrometry, assay reactions were separated by SDS-PAGE as described above, and gel bands corresponding to ubiquitinated USP30 excised. Proteins were then reduced, alkylated and digested with trypsin, using the Janus liquid handling system (PerkinElmer). The digests were subsequently analysed by LC-MS/MS on a Q-Exactive plus mass spectrometer, (ThermoScientific). LC-MS/MS data were searched against an in-house protein database using the Mascot search engine programme (Matrix Science)[22]. All data were interrogated manually.

USP30[c13]~Ub(F4R) was generated to assess the enzymatic activity of monoubiquitinated USP30. pParkin (4 μM) was incubated for 2 h at 37 ºC with USP30[c13] (4 μM) in the presence of human E1 (0.2 μM), UBE2L3 (2 μM), ubiquitin F4R (30 μM) and staurosporine (10 μM) in reaction buffer (20 mM Tris pH 8.5, 200 mM NaCl, 10 mM $MgCl_2$, 1 mM ATP, 0.7 mM DTT). Monoubiquitinated and free USP30 were partially separated through anion-exchange chromatography (Resource Q, 1 ml, GE Healthcare, buffers as during purification) and protein concentrations were determined through densitometry of Coomassie-stained gels of concentrated fractions that were subsequently assayed for Ub-KG-TAMRA cleavage activity as described above.

USP30(C77A)[c13]~Ub was generated to assess the effect of phosphoubiquitin on USP30 auto-deubiquitination. pParkin (4 μM) was incubated for 2 h at 37 ºC with USP30(C77A)[c13i] (4 μM) in the presence of human E1 (0.2 μM), UBE2L3 (2 μM), ubiquitin (30 μM) in reaction buffer (20 mM Tris pH 8.5, 200 mM NaCl, 10 mM $MgCl_2$, 1 mM ATP, 0.7 mM DTT). The reaction was then incubated with either GST-*Ph*PINK1 (2 μM) or with λ-phosphatase (6 μM), 1 mM $MnCl_2$ and staurosporine (10 μM) followed by incubation with Apyrase (NEB) and 5 mM $CaCl_2$. Samples were then buffer-exchanged into storage buffer (25 mM Tris pH 7.5, 150 mM NaCl, 5% (v/v) glycerol), 5 mM DTT), concentrated and incubated with USP30[c13] (0.25 μM) in PBS + 5 mM DTT for indicated times.

Disappearance of the USP30(C77A)^{c13}~(p)Ub species was followed by western blotting for USP30 as described above.

SEC-MALS

An Agilent 1200 Series chromatography system coupled to a DAWN Heleos II multi-angle light scattering detector as well as an Optilab rEX refractive index detector (Wyatt Technology) was used for size-exclusion chromatography multi-angle light scattering (SEC-MALS) analysis. Samples (100 μL of 2 mg/mL protein solutions) were run in PBS + 2 mM DTT with a flow of 0.5 mL/min on a Superdex 75 10/300 GL column (GE Healthcare). Masses and errors were derived from analysis in Astra 6.1 (Wyatt Technology) following calibration with BSA.

Isothermal titration calorimetry (ITC)

USP30^{c13i}, asymmetric Lys6-diUb* and wt Lys6-diUb were gel-filtrated into ITC buffer (25 mM Hepes pH 7.0, 100 mM NaCl, 1 mM TCEP) and subsequently concentrated in spin concentrators. ITC data were recorded on a MicroCal iTC200 system (GE Healthcare) at 25 ºC, with 13 μM USP30^{c13i} in the cell and 130 μM Lys6-diUb in the syringe. Data analysis with automated baseline correction and evaluation was carried out in OriginPro 8.5ITC and MicroCal PEAQ-ITC programs.

Thermal shift assay

Protein melting curves were recorded on a Corbett RG-6000 real time PCR cycler (30ºC to 85ºC with 7 s per 0.5 ºC). Samples contained 4 μM USP30 protein and 4x Sypro Orange in PBS + 5 mM DTT. Melting curves were obtained as the maxima of dF/dT versus T plots. All data were recorded in triplicate and in at least two independent experiments.

Ubiquitin chain phosphorylation and LC-MS analysis

Ubiquitin chains (final concentration: 10 μM) were phosphorylated by *Ph*PINK1 (1 μM) in 25 mM Tris pH 7.4, 150 mM NaCl, 10 mM MgCl$_2$, 10 mM ATP at 22 ºC. Reactions were quenched in 0.1% formic acid at indicated time points. Ub-KG-TAMRA (3 μM) was phosphorylated by *Ph*PINK1 (0.3 μM) as described above and dialysed overnight in PBS buffer. For USP treatment, wildtype Lys6-diUb and asymmetric Lys6-diUb (K6R and K48R in distal Ub moiety, K48R and ΔGly76 in proximal moiety, see Supplementary Fig. 11 and 12) were phosphorylated in 25 mM Tris pH 7.4, 150 mM NaCl, 10 mM MgCl$_2$, 1 mM ATP at 22 ºC and quenched by the addition of apyrase (5 U/100 μL) followed by heat inactivation of *Ph*PINK1 at 70 °C for 5 min. Precipitated protein was then removed by centrifugation. *Ph*PINK1-treated and untreated asymmetric Lys6-diUb was subjected to cleavage by USP21 (1 μM) at 22 ºC for 60 min and subsequently quenched in 0.1% formic acid. For LC-MS analysis, an Agilent 1200 Series chromatography system coupled to an Agilent 6130 Quadrupole mass spectrometer equipped with an ESI source was used. Samples were desalted on a Phenomenex Jupiter 5 μm 300 Å C4 column (150 x 2.0 mm) for 0.5 min at 5% buffer B (buffer A: water + 0.2% (v/v) formic acid, buffer B: acetonitrile + 0.2% (v/v) formic acid) followed by a linear gradient to 75% B over 10 min at 0.8 mL/min. Spectra were acquired in positive ion mode between m/z 400 and 2,000 (ionization voltage: 3 kV).

Averaged spectra were deconvoluted using Promass (Novatia, LLC). Time-course experiments were carried out in triplicate from three independent reactions. Homogeneously phosphorylated, asymmetric Lys6-diUb chains were obtained by phosphorylating K6R/K48R monoUb for the distal Ub moiety and K48R/?Gly76 monoUb for the proximal Ub moiety separately, and combining them with nonphosphorylated versions as appropriate for the assembly for asymmetric, distinctly phosphorylated Lys6-diUb* species. The phosphorylation was carried out as described above, the reaction mixture diluted in water, loaded onto a Mono Q 5/50 GL column (GE Healthcare) and eluted with a linear gradient into 50 mM Tris pH 7.5. Assembly of Lys6-diUb* was achieved by mixing the respective monoUb species in a 1:1 ratio in the presence of 0.22 μM mouse E1, 0.84 μM UbcH7, 0.9 μM NleL, 10 mM ATP, 40 mM Tris pH 7.5, 10 mM $MgCl_2$ and 0.6 mM DTT. Lys6-diUb* chains were purified on a Mono S 5/50 GL column (buffer A: 50 mM sodium acetate pH 4.5, buffer B: 50 mM sodium acetate pH 4.5, 1000 mM NaCl) and buffer exchanged in 3 kDa spin concentrators.

Cell-culture, pull-downs and immunoblotting

Inducible HeLa Flp-In T-REx cells expressing wild-type Parkin (gift from W. Harper, Harvard University) were cultured in DMEM + GlutaMAX supplemented with 10% (v/v) FCS and penicillin/streptomycin at 37°C in a humidified atmosphere containing 5% CO_2. Transcription of wild-type Parkin was induced with doxycycline (1 μg/mL) for 24 h prior to proteasome inhibition with MG-132 (10 μM, 2 h) or mitochondrial depolarisation with CCCP (10 μM, 1 h) as indicated. For USP30 knockdowns, cells were treated with 10 nM siGENOME Human USP30 (84749) siRNA (Dharmacon) complexed with Lipofectamine RNAiMAX (Life Technologies) according to the manufacturer's instruction for 16 h. Cells were harvested 72 h post knockdown. For USP30 overexpression, the full-length gene of codon-optimised USP30 followed by a stop codon was cloned into the pOPINE vector with mutations as indicated. Transfection was carried out using Lipofectamine LTX (DNA:Lipofectamine ratio 1:3) for 24 h, and cells were harvested 48 h post transfection. Cells were tested negative for mycoplasma contamination (Lonza MycoAlert™ Assay). A Life Sciences Reporting Summary for this article is available online.

Cells were washed with ice-cold PBS and incubated in lysis buffer (50 mM Tris pH 7.5, 150 mM NaCl, 2 mM EDTA, 5% (w/v) glycerol, 1% (v/v) NP-40, protease inhibitors (cOmplete EDTA-free protease inhibitor tablets, Roche), 10 mM chloroacetamide, supplemented with 6 μg GFP-tagged dimeric Lys6-affimer 42 per condition yielding ~ 6 mg of lysate) for 30 min at 4 ℃. Cells were harvested by scraping, and the lysate cleared by centrifugation (14,000 x g, 10 min, 4 ℃). Protein concentrations were measured by Bradford assays with BSA as a standard, allowing for equal amounts of cell lysate from each condition. The clear supernatant was incubated at 4 ℃ overnight, then supplemented with 13 μL of GFP-trap resin (Chromotek) and incubated for 2 h at 4 ℃ with over-head shaking. Beads were then washed three times in Co-IP buffer (50 mM Tris pH 7.5, 150 mM NaCl, 2 mM EDTA, 5% (w/v) glycerol, 1% (v/v) NP-40, 2 mM β-mercaptoethanol), incubated with 200 nM USP21 for 1 h at 4 ℃ and twice washed with Co-IP buffer. Proteins were eluted in SDS sample buffer at 95 ℃ for 5 min, separated by SDS-PAGE and analysed by Western blotting as described above. Primary antibodies recognised CISD1 (16006-1-AP, proteintech), GAPDH

(AM4300, Ambion), MIRO1 (HPA010687, Atlas Antibodies), Mitofusin 2 (ab56889, abcam), Parkin (ab77924, abcam), TOM20 (FL-145, sc-11414, Santa Cruz Biotechnology), Tubulin (clone DM1A, T6199, Sigma Aldrich), USP30 (HPA016952, Atlas Antibodies), VDAC1 (75-204, Neuromab). Clarity ECL Western Blotting Substrate (Bio-Rad) and SuperSignal West Femto Maximum Sensitivity Substrate (ThermoFisher) were used as ECL solutions.

Data availability and Accession Code Availability statements

A Life Sciences Reporting Summary for this article is available online. Lys6-specific affimer reagents can be obtained from Avacta (Wetherby, UK). Coordinates and structure factors have been deposited with the protein data bank under accession codes 5OHK, 5OHN, 5OHP. Uncropped images of all gels and western blots as well as raw data for gel-based kinetics experiments are shown in Supplementary Data Set 1. USP30 peptides identified by mass spectrometry following Parkin-mediated ubiquitination are presented in Supplementary Data Table 2.

Supplementary Material

Refer to Web version on PubMed Central for supplementary material.

Acknowledgments

References

1. Komander D, Rape M. The ubiquitin code. Annu Rev Biochem. 2012; 81:203–229. [PubMed: 22524316]

2. Hershko A, Ciechanover A. The ubiquitin system. Annu Rev Biochem. 1998; 67:425–479. [PubMed: 9759494]

3. Yau R, Rape M. The increasing complexity of the ubiquitin code. Cell Res. 2016; 18:579–586.

4. Swatek KN, Komander D. Ubiquitin modifications. Cell Res. 2016; 26:399–422. [PubMed: 27012465]

5. Pickrell AM, Youle RJ. The Roles of PINK1, Parkin, and Mitochondrial Fidelity in Parkinson's Disease. Neuron. 2015; 85:257–273. [PubMed: 25611507]

6. Nguyen TN, Padman BS, Lazarou M. Deciphering the Molecular Signals of PINK1/Parkin Mitophagy. Trends Cell Biol. 2016; 26:733–744. [PubMed: 27291334]

7. Kazlauskaite A, Muqit MMK. PINK1 and Parkin – mitochondrial interplay between phosphorylation and ubiquitylation in Parkinson's disease. FEBS J. 2015; 282:215–223. [PubMed: 25345844]

8. Narendra DP, et al. PINK1 is selectively stabilized on impaired mitochondria to activate Parkin. PLoS Biol. 2010; 8:e1000298. [PubMed: 20126261]

9. Kazlauskaite A, et al. Parkin is activated by PINK1-dependent phosphorylation of ubiquitin at Ser65. Biochem J. 2014; 460:127–139. [PubMed: 24660806]

10. Koyano F, et al. Ubiquitin is phosphorylated by PINK1 to activate parkin. Nature. 2014; 510:162–166. [PubMed: 24784582]

11. Kane LA, et al. PINK1 phosphorylates ubiquitin to activate Parkin E3 ubiquitin ligase activity. J Cell Biol. 2014; 205:143–153. [PubMed: 24751536]

12. Ordureau A, et al. Quantitative Proteomics Reveal a Feedforward Mechanism for Mitochondrial PARKIN Translocation and Ubiquitin Chain Synthesis. Mol Cell. 2014; 56:360–375. [PubMed: 25284222]

13. Wauer T, et al. Ubiquitin Ser65 phosphorylation affects ubiquitin structure, chain assembly and hydrolysis. EMBO J. 2015; 34:307–325. [PubMed: 25527291]

14. Wauer T, Simicek M, Schubert A, Komander D. Mechanism of phospho-ubiquitin-induced PARKIN activation. Nature. 2015; 524:370–374. [PubMed: 26161729]

15. Kazlauskaite A, et al. Binding to serine 65-phosphorylated ubiquitin primes Parkin for optimal PINK1-dependent phosphorylation and activation. EMBO Rep. 2015; 16:939–954. [PubMed: 26116755]

16. Sauvé V, et al. A Ubl/ubiquitin switch in the activation of Parkin. EMBO J. 2015; 34:2492–2505. [PubMed: 26254305]

17. Kumar A, et al. Disruption of the autoinhibited state primes the E3 ligase parkin for activation and catalysis. EMBO J. 2015; 34:2506–2521. [PubMed: 26254304]

18. Kondapalli C, et al. PINK1 is activated by mitochondrial membrane potential depolarization and stimulates Parkin E3 ligase activity by phosphorylating Serine 65. Open Biology. 2012; 2 120080.

19. Sarraf SA, et al. Landscape of the PARKIN-dependent ubiquitylome in response to mitochondrial depolarization. Nature. 2013; 496:372–376. [PubMed: 23503661]

20. Durcan TM, et al. USP8 regulates mitophagy by removing K6-linked ubiquitin conjugates from parkin. EMBO J. 2014; 33:2473–2491. [PubMed: 25216678]

21. Ordureau A, et al. Defining roles of PARKIN and ubiquitin phosphorylation by PINK1 in mitochondrial quality control using a ubiquitin replacement strategy. Proceedings of the National Academy of Sciences. 2015; 112:6637–6642.

22. Lazarou M, et al. The ubiquitin kinase PINK1 recruits autophagy receptors to induce mitophagy. Nature. 2015; 524:309–314. [PubMed: 26266977]

23. Heo J-M, Ordureau A, Paulo JA, Rinehart J, Harper JW. The PINK1-PARKIN Mitochondrial Ubiquitylation Pathway Drives a Program of OPTN/NDP52 Recruitment and TBK1 Activation to Promote Mitophagy. Mol Cell. 2015; 60:7–20. [PubMed: 26365381]

24. Pickrell AM, et al. Endogenous Parkin Preserves Dopaminergic Substantia Nigral Neurons following Mitochondrial DNA Mutagenic Stress. Neuron. 2015; 87:371–381. [PubMed: 26182419]

25. Corti O, Lesage S, Brice A. What genetics tells us about the causes and mechanisms of Parkinson's disease. Physiol Rev. 2011; 91:1161–1218. [PubMed: 22013209]

26. Mevissen TET, Komander D. Mechanisms of Deubiquitinase Specificity and Regulation. Annu Rev Biochem. 2017; 86:159–192. [PubMed: 28498721]

27. Clague MJ, et al. Deubiquitylases from genes to organism. Physiol Rev. 2013; 93:1289–1315. [PubMed: 23899565]

28. Cornelissen T, et al. The deubiquitinase USP15 antagonizes Parkin-mediated mitochondrial ubiquitination and mitophagy. Hum Mol Genet. 2014; 23:5227–5242. [PubMed: 24852371]

29. Bingol B, et al. The mitochondrial deubiquitinase USP30 opposes parkin-mediated mitophagy. Nature. 2014; 510:370–375. [PubMed: 24896179]

30. Liang J-R, et al. USP30 deubiquitylates mitochondrial Parkin substrates and restricts apoptotic cell death. EMBO Rep. 2015; 16:618–627. [PubMed: 25739811]

31. Cunningham CN, et al. USP30 and parkin homeostatically regulate atypical ubiquitin chains on mitochondria. Nature Cell Biology. 2015; 17:160–169. [PubMed: 25621951]

32. Wang Y, et al. Deubiquitinating enzymes regulate PARK2-mediated mitophagy. Autophagy. 2015; 11:595–606. [PubMed: 25915564]

33. Nakamura N, Hirose S. Regulation of mitochondrial morphology by USP30, a deubiquitinating enzyme present in the mitochondrial outer membrane. Mol Biol Cell. 2008; 19:1903–1911. [PubMed: 18287522]

34. Urbé S, et al. Systematic survey of deubiquitinase localization identifies USP21 as a regulator of centrosome- and microtubule-associated functions. Mol Biol Cell. 2012; 23:1095–1103. [PubMed: 22298430]

35. Elia AEH, et al. Quantitative Proteomic Atlas of Ubiquitination and Acetylation in the DNA Damage Response. Mol Cell. 2015; 59:867–881. [PubMed: 26051181]

36. Lin DY-W, Diao J, Zhou D, Chen J. Biochemical and structural studies of a HECT-like ubiquitin ligase from Escherichia coli O157:H7. J Biol Chem. 2011; 286:441–449. [PubMed: 20980253]

37. Hospenthal MK, Freund SMV, Komander D. Assembly, analysis and architecture of atypical ubiquitin chains. Nat Struct Mol Biol. 2013; 20:555–565. [PubMed: 23563141]

38. Faesen AC, et al. The differential modulation of USP activity by internal regulatory domains, interactors and eight ubiquitin chain types. Chem Biol. 2011; 18:1550–1561. [PubMed: 22195557]

39. Ritorto MS, et al. Screening of DUB activity and specificity by MALDI-TOF mass spectrometry. Nature Communications. 2014; 5:4763.

40. Yue W, et al. A small natural molecule promotes mitochondrial fusion through inhibition of the deubiquitinase USP30. Cell Res. 2014; 24:482–496. [PubMed: 24513856]

41. Bingol B, Sheng M. Mechanisms of mitophagy: PINK1, Parkin, USP30 and beyond. Free Radic Biol Med. 2016; 100:210–222. [PubMed: 27094585]

42. Michel MA, Swatek KN, Hospenthal MK, Komander D. Ubiquitin linkage-specific affimers reveal insights into K6-linked ubiquitin signaling. Mol Cell. 2017

43. Ye Y, Scheel H, Hofmann K, Komander D. Dissection of USP catalytic domains reveals five common insertion points. Mol Biosyst. 2009; 5:1797–1808. [PubMed: 19734957]

44. Ekkebus R, et al. On terminal alkynes that can react with active-site cysteine nucleophiles in proteases. J Am Chem Soc. 2013; 135:2867–2870. [PubMed: 23387960]

45. Hu M, et al. Crystal structure of a UBP-family deubiquitinating enzyme in isolation and in complex with ubiquitin aldehyde. Cell. 2002; 111:1041–1054. [PubMed: 12507430]

46. Ye Y, et al. Polyubiquitin binding and cross-reactivity in the USP domain deubiquitinase USP21. EMBO Rep. 2011; 12:350–357. [PubMed: 21399617]

47. Renatus M, et al. Structural basis of ubiquitin recognition by the deubiquitinating protease USP2. Structure. 2006; 14:1293–1302. [PubMed: 16905103]

48. Komander D, et al. Molecular discrimination of structurally equivalent Lys 63-linked and linear polyubiquitin chains. EMBO Rep. 2009; 10:466–473. [PubMed: 19373254]

49. Komander D, et al. The structure of the CYLD USP domain explains its specificity for Lys63-linked polyubiquitin and reveals a B box module. Mol Cell. 2008; 29:451–464. [PubMed: 18313383]

50. Sato Y, et al. Structures of CYLD USP with Met1- or Lys63-linked diubiquitin reveal mechanisms for dual specificity. Nat Struct Mol Biol. 2015; 22:222–229. [PubMed: 25686088]

51. Okatsu K, et al. Phosphorylated ubiquitin chain is the genuine Parkin receptor. J Cell Biol. 2015; 209:111–128. [PubMed: 25847540]

52. Dong X, et al. Ubiquitin S65 phosphorylation engenders a pH-sensitive conformational switch. Proceedings of the National Academy of Sciences. 2017; 114:6770–6775.

53. Kim W, et al. Systematic and quantitative assessment of the ubiquitin-modified proteome. Mol Cell. 2011; 44:325–340. [PubMed: 21906983]

54. Wagner SA, et al. A proteome-wide, quantitative survey of in vivo ubiquitylation sites reveals widespread regulatory roles. Mol Cell Proteomics. 2011; 10 M111.013284.

55. Newton K, et al. Ubiquitin chain editing revealed by polyubiquitin linkage-specific antibodies. Cell. 2008; 134:668–678. [PubMed: 18724939]

56. Matsumoto ML, et al. K11-linked polyubiquitination in cell cycle control revealed by a K11 linkage-specific antibody. Mol Cell. 2010; 39:477–484. [PubMed: 20655260]

57. Matsumoto ML, et al. Engineering and structural characterization of a linear polyubiquitin-specific antibody. J Mol Biol. 2012; 418:134–144. [PubMed: 22227388]

58. Berrow NS, et al. A versatile ligation-independent cloning method suitable for high-throughput expression screening applications. Nucleic Acids Res. 2007; 35:e45. [PubMed: 17317681]

59. Higuchi R, Krummel B, Saiki RK. A general method of in vitro preparation and specific mutagenesis of DNA fragments: study of protein and DNA interactions. Nucleic Acids Res. 1988; 16:7351–7367. [PubMed: 3045756]

60. Faggiano S, Alfano C, Pastore A. The missing links to link ubiquitin: Methods for the enzymatic production of polyubiquitin chains. Anal Biochem. 2016; 492:82–90. [PubMed: 26470940]

61. Wilkinson KD, Gan-Erdene T, Kolli N. Derivitization of the C-terminus of ubiquitin and ubiquitin-like proteins using intein chemistry: methods and uses. Meth Enzymol. 2005; 399:37–51. [PubMed: 16338347]

62. Kabsch W. XDS. Acta Crystallogr D Biol Crystallogr. 2010; 66:125–132. [PubMed: 20124692]

63. Waterman DG, et al. Diffraction-geometry refinement in the DIALS framework. Acta Crystallogr D Struct Biol. 2016; 72:558–575. [PubMed: 27050135]

64. Evans P. Scaling and assessment of data quality. Acta Crystallogr D Biol Crystallogr. 2006; 62:72–82. [PubMed: 16369096]

65. McCoy AJ, et al. Phaser crystallographic software. J Appl Crystallogr. 2007; 40:658–674. [PubMed: 19461840]

66. Stein, N. J Appl Crystallogr. Vol. 41. IUCr; 2008. CHAINSAW: a program for mutating pdb files used as templates in molecular replacement; p. 641-643.

67. Vijay-Kumar S, Bugg CE, Cook WJ. Structure of ubiquitin refined at 1.8 A resolution. J Mol Biol. 1987; 194:531–544. [PubMed: 3041007]

68. Nicholls RA, Fischer M, McNicholas S, Murshudov GN. Conformation-independent structural comparison of macromolecules with ProSMART. Acta Crystallogr D Biol Crystallogr. 2014; 70:2487–2499. [PubMed: 25195761]

69. Emsley P, Lohkamp B, Scott WG, Cowtan K. Features and development of Coot. Acta Crystallogr D Biol Crystallogr. 2010; 66:486–501. [PubMed: 20383002]

70. Adams PD, et al. The Phenix software for automated determination of macromolecular structures. Methods. 2011; 55:94–106. [PubMed: 21821126]

71. Murshudov GN, et al. REFMAC5 for the refinement of macromolecular crystal structures. Acta Crystallogr D Biol Crystallogr. 2011; 67:355–367. [PubMed: 21460454]

72. Silva JC, et al. Quantitative proteomic analysis by accurate mass retention time pairs. Anal Chem. 2005; 77:2187–2200. [PubMed: 15801753]
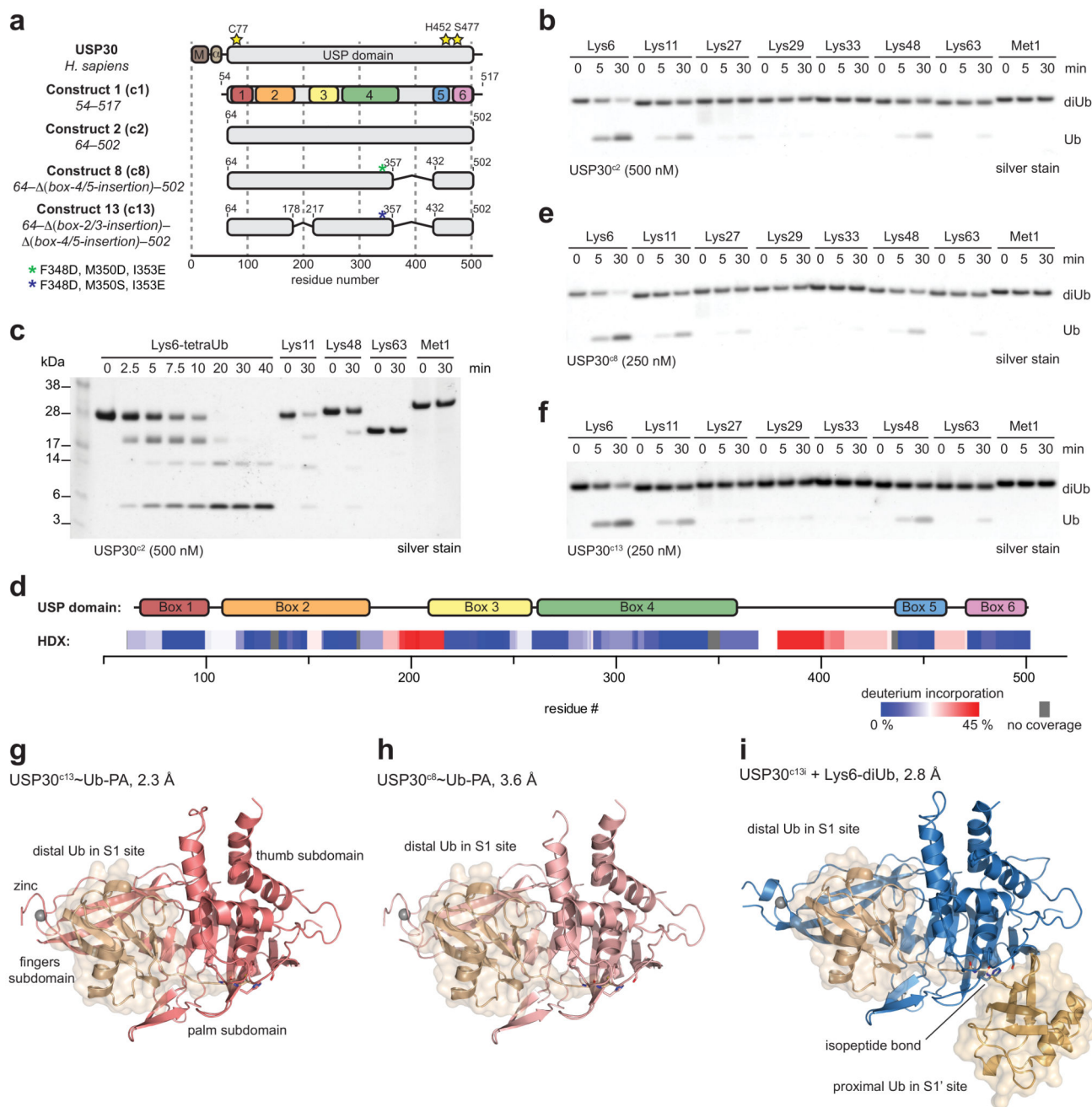
**Figure 1. Linkage preference, construct optimisation and structures of USP30.**
a, Constructs of human USP30 used in this study. The mitochondrial intermembrane part (M), the transmembrane helix (α), the catalytic residues and the annotation of boxes of the cytosolic USP domain43 are indicated. Also see Supplementary Table 1. **b,** Time course analysis of indicated diubiquitin cleavage with USP30 catalytic domain (construct 2, USP30^{c2}) resolved by SDS-PAGE and visualised by silver staining. **c,** Tetraubiquitin cleavage analysis as in **b**. Gels in **b** and **c** are representative of triplicate experiments. Also see Supplementary Fig. 1a-b. **d,** Deuterium incorporation obtained from HDX-MS for

USP30^{c2}, indicating flexible parts (red) in the insertions between USP boxes 2 and 3, and 4 and 5. Also see Supplementary Fig. 1c-e. **e,f,** Specificity analysis as in **b** for indicated USP30 constructs lacking insertions (compare **a**), representative of duplicate experiments. **g,h,i,** Cartoon representation of covalent USP30^{c13}~Ub-PA (2.3 Å, *left*), USP30^{c8}~Ub-PA (3.6 Å, *middle*) and inactive USP30^{c13} C77A noncovalently bound to Lys6-diubiquitin (USP30^{c13i}-Lys6-diUb, 2.8 Å, *right*). Ubiquitin molecules are shown with transparent surfaces. See Supplementary Fig. 3 and Table 1. Uncropped images for gels are shown in Supplementary Data Set 1.
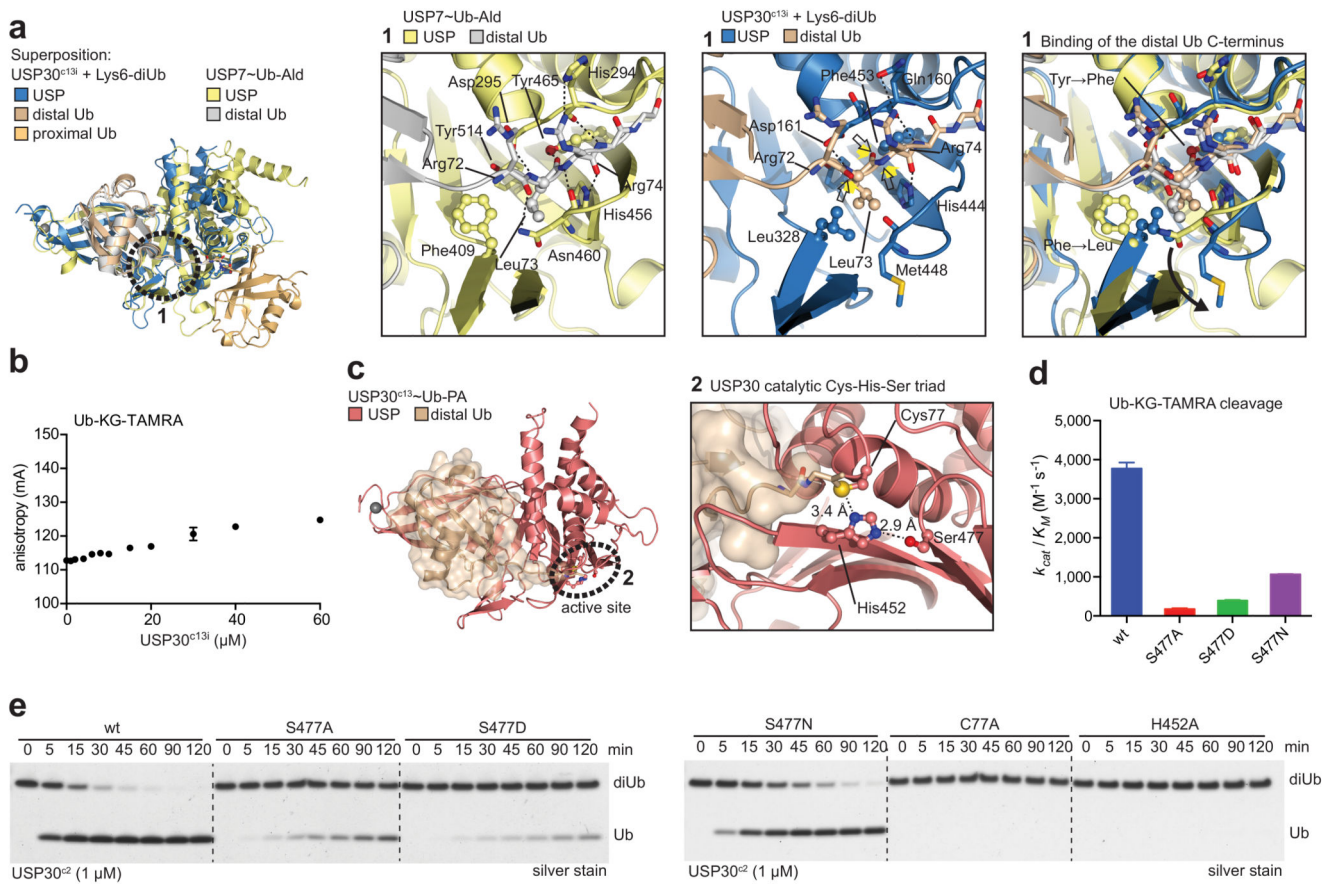
**Figure 2. USP30 employs a Cys-His-Ser catalytic triad.**

a, Superposition of the USP30 diubiquitin complex (blue/orange) with the USP7~ubiquitin aldehyde complex (yellow/grey, PDB 1NBF45). Close-up views focus on coordination of the distal ubiquitin C-terminus with hydrogen bonds as black dotted lines. Yellow arrows indicate lost hydrogen bonds in USP30 due to indicated amino acid changes. **b,** Fluorescence polarisation binding experiment of USP30^{c13i} to ubiquitin-KG-TAMRA, indicating weak binding. Experiments were performed in triplicate and errors represent standard deviation from the mean. **c,** Cartoon representation of the USP30^{c13}~Ub-PA complex and close-up view of the catalytic triad. **d,** Catalytic efficiencies (k_{cat}/K_M) for Ser477 mutant proteins derived from a ubiquitin-KG-TAMRA cleavage assay, see Supplementary Fig. 5e-f. Experiments were performed in triplicate and error bars indicate standard error. **e,** Lys6-diubiquitin cleavage assay for indicated USP30 mutants, performed in duplicate. Uncropped images for gels are shown in Supplementary Data Set 1.
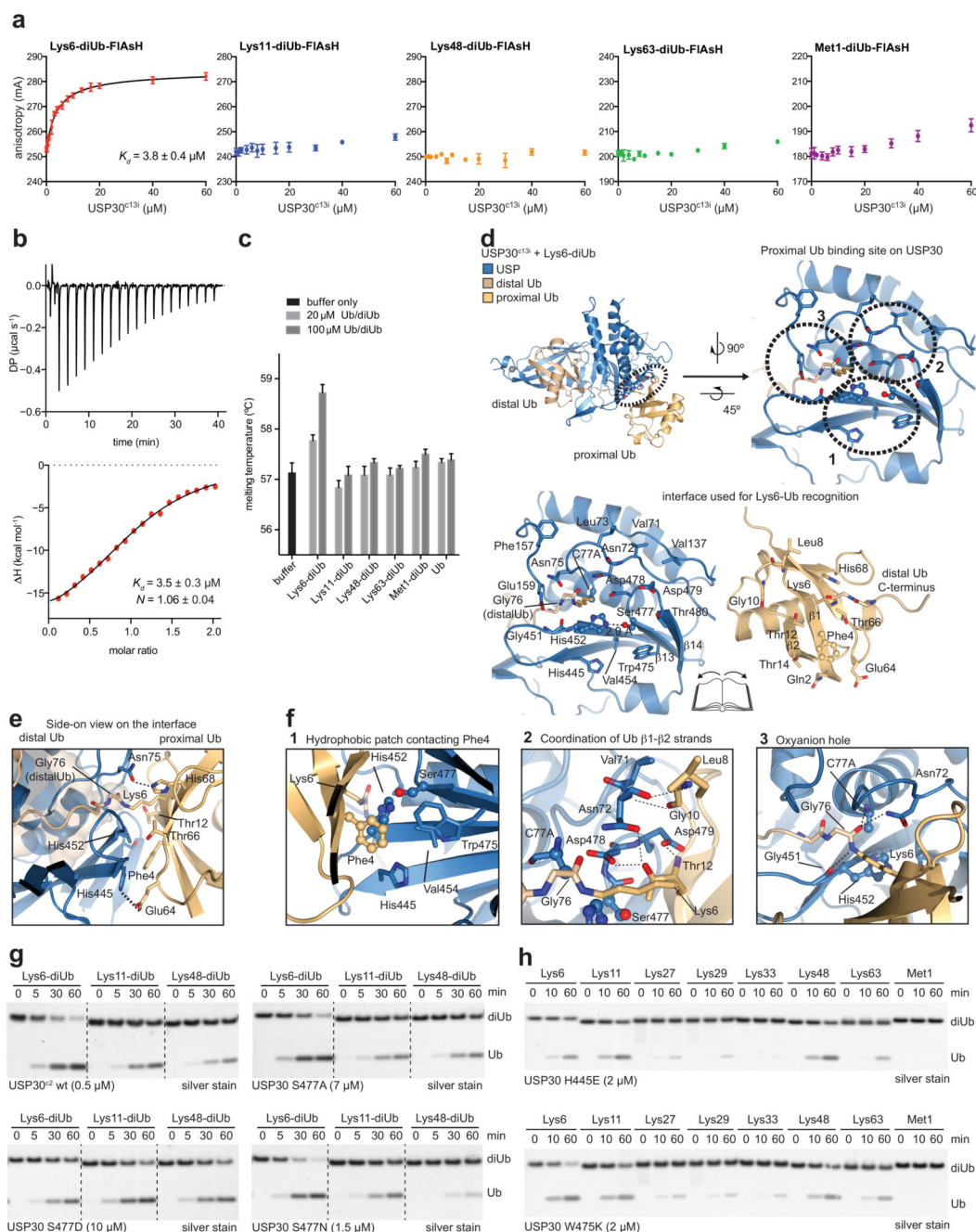
Figure 3. A Lys6-specific proximal ubiquitin binding site in USP30 explains linkage preference.
**a,** Fluorescence polarisation binding experiment with FlAsH-tagged diubiquitins and inactive USP30^{c13i}. Experiments were performed in triplicate and errors represent standard deviation from the mean. **b,** Isothermal titration calorimetry (ITC) data for Lys6-diubiquitin binding to USP30^{c13i}. **c,** Melting curve analysis of USP30^{c13i} in the absence (black bar) or presence (grey bars) of indicated ubiquitin species, showing concentration dependent stabilisation by Lys6- but not other diubiquitin molecules or monoubiquitin. This supports specific binding to Lys6-linked diubiquitin, also for unlabelled ubiquitin species. Mean ±

standard error from three independent measurements. **d,** Cartoon representation of the USP30 Lys6-diubiquitin complex. The interface highlighted with a black circle is presented in open-book view in the figures to the right. Residues involved in the interaction are labelled. **e,** Side-on view of the interface. **f,** Close-up views on three sections of the interface (dotted lines in **d**): 1, Ubiquitin Phe4 patch binding to a hydrophobic USP30 surface near the catalytic triad. 2, Ubiquitin β1-β2 loop coordination by the USP30 thumb and palm domains. 3, Ubiquitin Lys6 interaction within the catalytic centre near the oxyanion hole (Cys77 and Asn72). **g,** Diubiquitin cleavage assay with indicated substrates and Ser477 mutants, titrated to similar activity levels. Also see Supplementary Fig. 6g, h. **h,** Diubiquitin specificity assay as in Fig. 1b with USP30 mutants in the proximal binding site (W475K or H445E) that abrogate specificity. Gel-based assays in **g** and **h** were performed in triplicate and duplicate, respectively. Uncropped images for gels are shown in Supplementary Data Set 1.
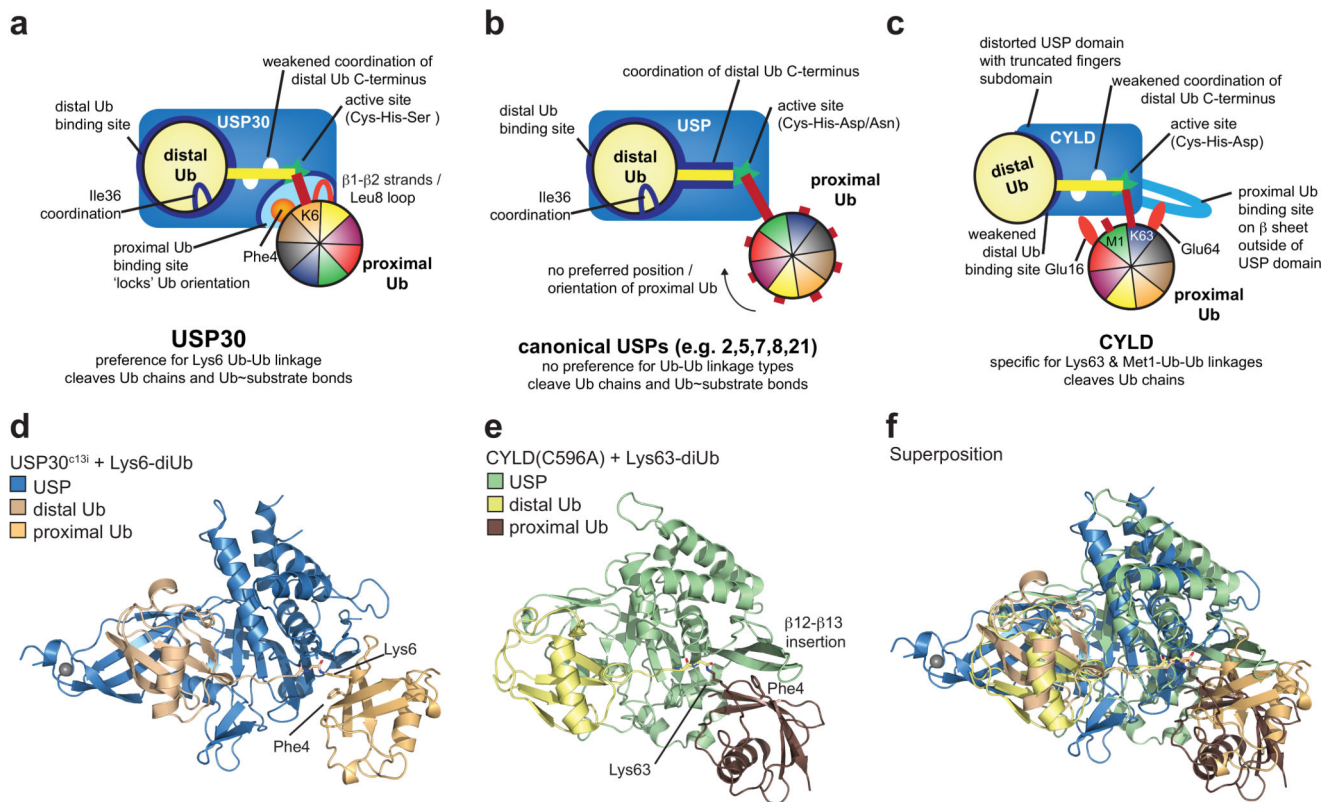
Figure 4. Mechanisms of USP linkage specificity.
a, Model for specific recognition of the proximal Ub moiety of Lys6-diUb by USP30. **b,** Most canonical USP domains require no preferred orientation of the proximal Ub for efficient catalysis. **c,** The truncated USP domain of CYLD contains a weakened distal Ub binding site. An inserted β-sheet outside of the catalytic domain positions Lys63- and Met1-linked chains for specific processing of these chain types. This mechanism of linkage selection is distinct from USP30 where recognition of the proximal Ub is achieved through a binding site contained within palm subdomain. **d,** Structure of USP30^{c13i}-Lys6-diUb. **e,** Cartoon representation of the Lys63/Met1-specific USP enzyme CYLD, in its inactive (C596A) form with Lys63-diubiquitin bound 50 (PDB ID: 3WXG). **f,** Superposition of **d** and **e** shows the different arrangements of both the distal and the proximal ubiquitin moieties. Lack of the fingers subdomain enables a shifted binding mode for the distal ubiquitin also encompassing a differently coordinated C-terminal tail. See also Supplementary Fig. 9.
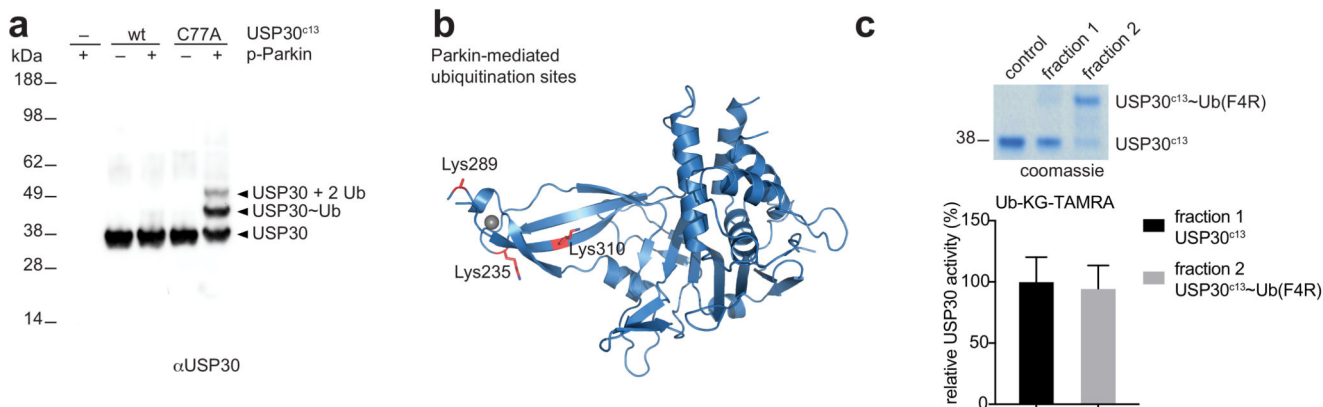
Figure 5. Monoubiquitination of USP30 by Parkin does not affect its catalytic activity.
**a,** *In vitro* reconstitution of USP30^{c13} ubiquitination by phosphorylated Parkin, visualised by western blotting for USP30. Active USP30 can auto-deubiquitinate in trans. **b,** USP30 ubiquitination sites found by mass spectrometry (Supplementary Data Table 2) match annotated sites in cell lines[29,31] and cluster at the tip of the Fingers subdomain. **c,** Active USP30^{c13} was modified by Parkin with ubiquitin F4R that prevents auto-deubiquitination. Free and modified forms were separated by ion-exchange chromatography, quantified by densitometry and their activities determined in ubiquitin-KG-TAMRA assays (triplicate measurements, values represent mean with standard error). See also Supplementary Fig. 10. Uncropped images for gels are shown in Supplementary Data Set 1.
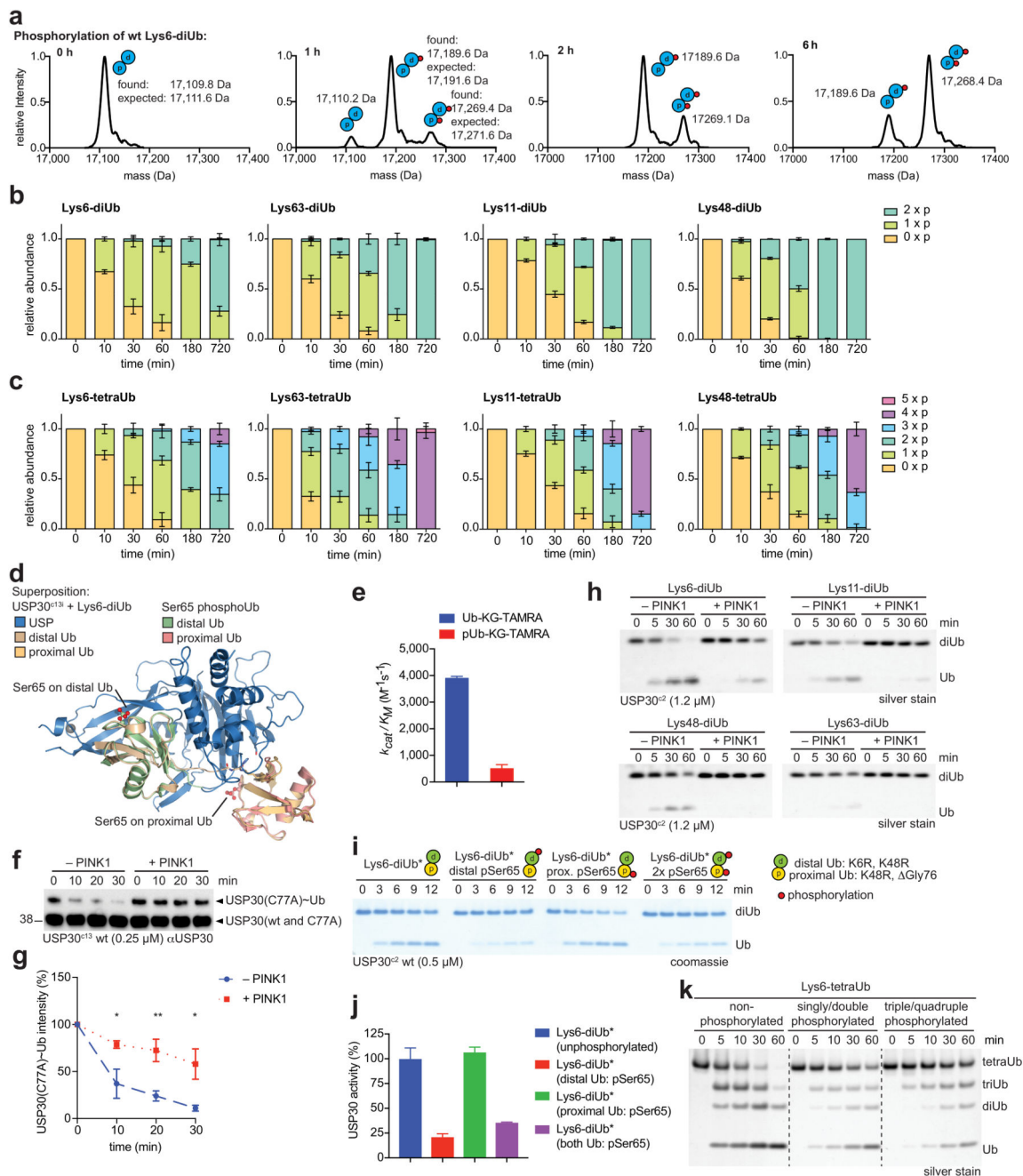
Figure 6. Indirect regulation of USP30 activity through PINK1-mediated phosphorylation of ubiquitin.

a, Deconvoluted mass spectra of a wild-type Lys6-diubiquitin phosphorylation time course, showing biphasic phosphorylation kinetics. **b,c,** Time course analysis of ubiquitin chain phosphorylation. Ubiquitin chains (dimers in **b**, tetramers in **c**) were incubated with *Ph*PINK113 for indicated times and their phosphorylation status was quantified by intact protein mass spectrometry. Mean ± s.d. of triplicate experiments. **d,** Superposition of the structure of Ser65-phosphorylated ubiquitin (PDB 4WZP13) on the proximal and distal

ubiquitin in the USP30 Lys6-diubiquitin complex places the phosphate groups at USP30-ubiquitin interfaces. See Supplementary Fig. 11b for a close-up. **e,** Catalytic efficiencies of USP30^{c2} for Ub-KG-TAMRA and phosphoUb-KG-TAMRA substrates. Experiments were performed in triplicate and standard error is indicated. **f,** USP30^{c13i} was ubiquitinated by Parkin as in Fig. 5a, optionally incubated with *Ph*PINK1, and treated with active USP30^{c13} for indicated times. Depletion of the USP30^{c13i}~Ub band was followed by western blotting for USP30. **g,** Quantification from four independent experiments as in **i**. Values represent mean with standard error of the mean. Two-sided ANOVA (F = 12) with Bonferroni's correction. *, $P < 0.05$; **, $P < 0.01$. **h,** Diubiquitin cleavage experiment with doubly phosphorylated diubiquitins of indicated linkages. Ubiquitin phosphorylation impairs USP30 activity for all chain types. **i,** Lys6-diubiquitin cleavage assay with nonphosphorylated, singly phosphorylated and doubly phosphorylated, asymmetric diubiquitin. See Supplementary Fig. 11a and 12a for substrate characterisation data. **j,** Quantification from gel-based kinetics shown in **i**. Error bars represent standard deviations from the mean of four independent experiments. **k,** Cleavage assay with unphosphorylated, singly (90%)/doubly(10%) phosphorylated and triply (60%)/quadruply (40%) phosphorylated Lys6-tetraubiquitin substrates. Uncropped images for gels are shown in Supplementary Data Set 1.
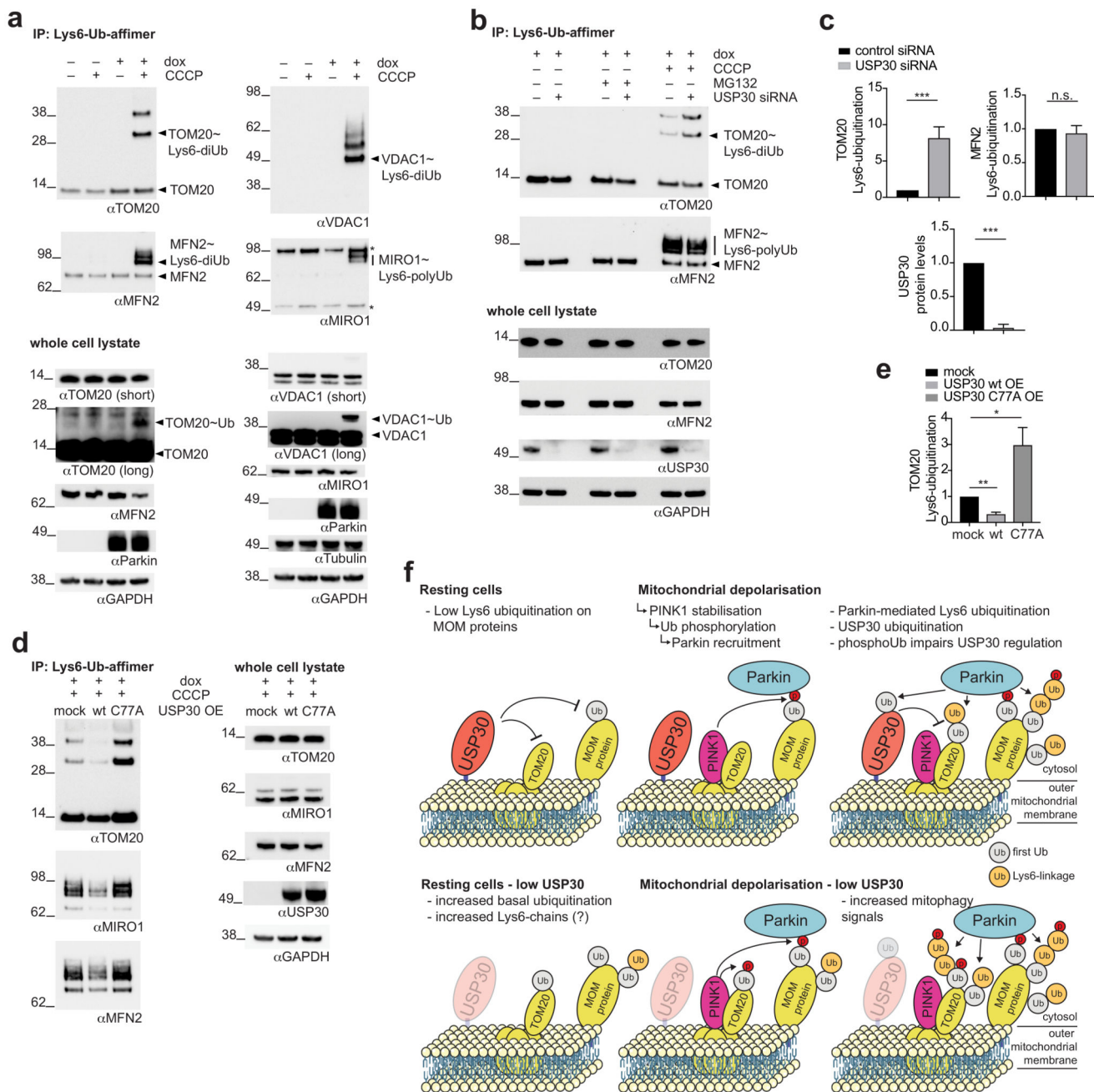
Figure 7. Lys6-linked polyubiquitin chains are assembled by Parkin on TOM20 during mitophagy and are regulated by USP30.

a, Immunoblotting for TOM20, VDAC1, MFN2 and MIRO1 in eluates of Lys6-linked polyubiquitin chain pull-downs from HeLa Flp-In T-REx cells, dox-inducibly expressing wild-type Parkin. Cells were treated as indicated. Affimer binding protects Lys6-linkages, but not other chain types, from USP21 cleavage42. All eluates were treated with USP21 to deplete other polyubiquitin linkages. For TOM20, short and long exposures are shown of the same samples but on different gels. *, non-specific bands. **b**, Experiment as in **a** with USP30 knock-down. **c**. Quantification from **b**. Mean ± s.e.m. Wilcoxon-Mann-Whitney test from n

= 3 (top and middle), n = 4 (bottom) independent experiments. ***, $P < 0.001$; n.s., non-significant. **d**, Experiment as in **a** with USP30 overexpression as indicated via transient transfection. **e,** Quantification from **d**. Mean ± s.e.m. One-Way ANOVA ($F = 7.6$) with Dunnett's correction, n = 4 independent experiments. *, $P < 0.05$; **, $P < 0.01$. **f,** Model for the regulation of mitochondrial protein ubiquitination by USP30 during mitophagy. Uncropped images for gels are shown in Supplementary Data Set 1.

Table 1

Data collection and refinement statistics.

	USP30^{c8} ~Ub-PA (PDB code: 5OHN)	USP30^{c13}~Ub-PA (PDB code: 5OHK)	USP30^{c13i} + Lys6-diUb (PDB code: 5OHP)
Data collection			
Space group	$P6_5$	$P2_122_1$	$P6_522$
Cell dimensions			
a, b, c (Å)	181.83, 181.83, 94.96	50.92, 94.41, 96.12	117.50, 117.50, 138.84
α, β, γ (°)	90, 90, 120	90, 90, 90	90, 90, 120
Resolution (Å)	157.5 – 3.60 (3.94 – 3.60)	67.35 – 2.34 (2.42 – 2.34)	82.08 – 2.80 (2.90 – 2.80)
R_{merge}	0.124 (0.900)	0.170 (0.715)	0.170 (0.998)
R_{meas}	0.144 (1.044)	0.194 (0.814)	0.192 (1.122)
$I/\sigma(I)$	10.0 (1.9)	4.6 (1.9)	7.0 (1.8)
$CC_{1/2}$	0.997 (0.593)	0.983 (0.848)	0.990 (0.714)
Completeness (%)	99.3 (99.6)	99.7 (99.1)	99.2 (99.9)
Redundancy	7.0 (7.2)	4.2 (4.0)	4.7 (4.8)
Refinement			
Resolution (Å)	3.6 Å	2.3 Å	2.8 Å
No. reflections	19801	20054	14379
R_{work} / R_{free}	21.1 / 25.2	22.6 / 26.0	21.6 / 24.7
No. atoms	5789	3017	3731
Protein	5787	2934	3678
Zinc	2	1	1
Water	0	82	52
B factors	165.7	42.8	47.5
Protein	165.7	42.7	47.6
Zinc	111.8	96.6	65.1
Water	-	43.6	42.3
R.m.s. deviations			
Bond lengths (Å)	0.020	0.003	0.007
Bond angles (°)	1.62	0.52	0.75

Each dataset was collected from a single crystal. Values in parentheses are for highest-resolution shell.